Growth rate effects on the thermoelectric performance of $CaMnO_3$-based ceramics

N.M. Ferreira[1,2], N.R. Neves[1], M.C. Ferro[2], M. A. Torres[3], M. A. Madre[3], F.M. Costa[1], A. Sotelo[3], A.V. Kovalevsky[2]

[1]I3N, Physics Department, University of Aveiro, 3810-193 Aveiro, Portugal

[2] CICECO - Aveiro Institute of Materials, Department of Materials and Ceramic Engineering, University of Aveiro, 3810-193 Aveiro, Portugal

[3] ICMA, CSIC-Universidad de Zaragoza, Zaragoza, Spain

*corresponding author: nmferreira@ua.pt

Abstract

$CaMnO_3$–based materials represent a promising family of n-type oxide thermoelectrics. The objective of the present work is assessing the impacts on relevant structural, microstructural and thermoelectric properties of manganites when they are processed by the laser floating zone technique. For this purpose, donor-doped $Ca_{0.9}La_{0.1}MnO_3$, $CaMn_{0.95}Nb_{0.05}O_3$ and undoped $CaMnO_3$ were used. Different growth conditions have been evaluated through combined studies of structural, microstructural, and thermoelectric characteristics. Despite the presence of secondary phases, electrical resistivity is among the best reported in the literature (9 mΩ.cm at 800ºC for La-doped materials grown at 200 mm/h). Essentially high absolute Seebeck coefficient of 320 μV/K at 800ºC was observed for undoped samples grown at 10 mm/h. Power factor is significantly affected by the growth conditions, reaching the highest values when using the lowest pulling rates. Exceptionally high PF (0.39 mW/K^{2}m at 800ºC) was obtained for undoped $CaMnO_3$ samples grown at 10 mm/h.

Keywords:

Oxide thermoelectrics, calcium manganite, laser processing, thermoelectric performance, electrical properties

Introduction

Nowadays most of the world electricity production implies the use of fossil fuels, characterized by the relatively low efficiencies of these systems (about 30-35 %) [1]. Consequently, there are large energy losses in form of heat, and enormous greenhouse gas generation. Moreover, the combustion engines used in the automotive sector also operate with low efficiency (~ 20-25 %) [2], leading to the same drawbacks. With the objective of decreasing the use of fossil fuels and corresponding negative impacts on the society and environment, the research in thermoelectric materials (TE) can lead, at least, to a partial solution of this problematic issue. TE devices represent an alternative to produce low-cost energy from the wasted heat. Furthermore, they have a long useful life and, in most of cases, they are environmentally friendly. Thermoelectric modules for energy harvesting have good prospects for the applications in military sector, automotive and aerospace industry, mostly for specific purposes. However, these modules are typically based on Bi_2Te_3 and Sb_2Te_3 compounds, with efficiencies of 4-5% [3], and composed of toxic and rare elements. Moreover, their chemical stability impedes the operation in air at even moderately elevated temperatures.

Due to these constraints, the scientific community emphasized its efforts in searching for alternative materials, as oxides [3,4]. These materials are chemically more stable, possess considerably lower toxicity, are cheaper, and can be used at high temperatures, increasing the Carnot efficiency. Consequently, they are very favourable for practical applications, when harvesting heat from high temperature sources [5,6]. Among these oxides, perovskite-type calcium manganite, $CaMnO_3$, represents a very promising n-type thermoelectric material [4,7]. On the other hand, $CaMnO_3$ possesses the main drawback of all oxide materials, namely, relatively low conversion efficiency. As a result, many research works have been performed to improve the thermoelectric properties of this compound, through doping [6], and/or different processing techniques [8-10]. Specific challenges related to calcium manganite include low mechanical strength, possibility of phase modifications occurring at around 900 ºC, and the appearance of oxygen-rich areas when the precursors are not homogeneous [11].

The main studies performed on this compound are essentially focused on the improvement of its electrical conductivity (σ), which is usually very low in the pure compound, without drastic modifications of Seebeck coefficient (S) or thermal conductivity (κ). Electron doping has demonstrated its suitability to increase electrical conductivity and, simultaneously, reduce thermal conductivity through lattice defects promoted by the dopant [12-14]. The final objective is, evidently, raising the thermoelectric performance of these materials, which is usually evaluated through the so-called dimensionless Figure-of-Merit (ZT): $ZT = \sigma*S^2*T/\kappa$. Most of the available works in the literature are focused on single-doping approaches to improve the thermoelectric performance of $CaMnO_3$. However, other promising approaches should be considered, as co-doping, nanostructuring, and/or nanocomposite fabrication, which also represent promising pathways to dramatically enhance ZT [5,7,14,15].

This work explores the possibility to process calcium manganite-based thermoelectric materials through the laser floating zone (LFZ) method. To the best of our knowledge, this is the first attempt to apply this technique for processing thermoelectric manganites. For this purpose, lanthanum and niobium oxides have been used as dopants due to their different substitution mechanism in the $CaMnO_3$ network [16]. Lanthanum is known to replace some of the A-site calcium ions, while niobium replaces B-site manganese ions [16]. Besides their donor effects, the induced structure modification is known to decrease thermal conductivity [16]. Moreover, undoped $CaMnO_3$ has also been prepared in the same conditions to be used as a reference. The samples were processed using the LFZ method at different pulling rates, from 10 to 200 mm/h. Structural, microstructural, and thermoelectric characterization (evaluated through the power factor, $PF=S^2/\rho$; ρ: electrical resistivity) have been performed in order to understand the effect produced by the pulling rates and dopants.

Experimental procedure

$CaCO_3$ (Merck, 99%), MnO_2 (Aldrich, 99%), La_2O_3 (Aldrich, 99.99%), and Nb_2O_5 (Aldrich, 99%) commercial powders were weighed in stoichiometric proportions to prepare the following compounds: $CaMnO_3$ (CMO), $Ca_{0.9}La_{0.1}MnO_3$ (CLMO),

and $CaMn_{0.95}Nb_{0.05}O_3$ (CMNO). These powders were then milled and mixed with polyvinyl alcohol (PVA), used as an organic binder to produce 150 mm long and 3 mm diameter cylindrical bars through extrusion [17,18] which were subsequently dried under air. After drying, the rods were used as feed and seed in a LFZ system described elsewhere [19]. The samples were processed using a continuous CO_2 Spectron SLC laser (λ = 10.6 µm, and power up to 200 W) under air at 10, 50, 100 and 200 mm/h growth rates to understand their effect on the structural, microstructural, and thermoelectric behaviour of these compounds.

Structural analysis has been performed using powder X-ray diffraction (XRD) in a Panalytical X'pert PRO3 diffractometer (CuKα1 radiation). The obtained spectra were analyzed using the JCPDS database. Microstructure has been studied on polished longitudinal sections of samples through scanning electron microscopy (SEM) in a Vega 3 from Tescan with an EDS Bruker system to determine the qualitative composition of the different phases. Samples density was measured by the Archimedes method at room temperature, using 4.71 g/cm^3 as the theoretical one for $CaMnO_3$ [20].

Thermoelectric behaviour of samples has been studied by simultaneous measurement of electrical resistivity and Seebeck coefficient, using the four point method, between 50 and 800 ºC in a LSR-3 device (Linseis GmbH). Power factor was then calculated using these data to determine the samples performances.

Results

Representative powder XRD patterns of samples after LFZ processing are displayed in Fig. 1. The orthorhombic perovskite-type phase $CaMnO_3$ (00-050-1746) can be observed in all samples as the major one. However, $CaMn_2O_4$ (01-074-2293, marokite) and tetragonal $Ca_3Mn_2O_7$ (00-041-0421) secondary phases have also been detected, in agreement with previous observations for this system [8,10,16,21-23]. On the other hand, the amount of secondary phases in CLMO and CMNO decreases when lower growth rates are used, since slower growth facilitates the formation of the thermodynamically-favoured phases.

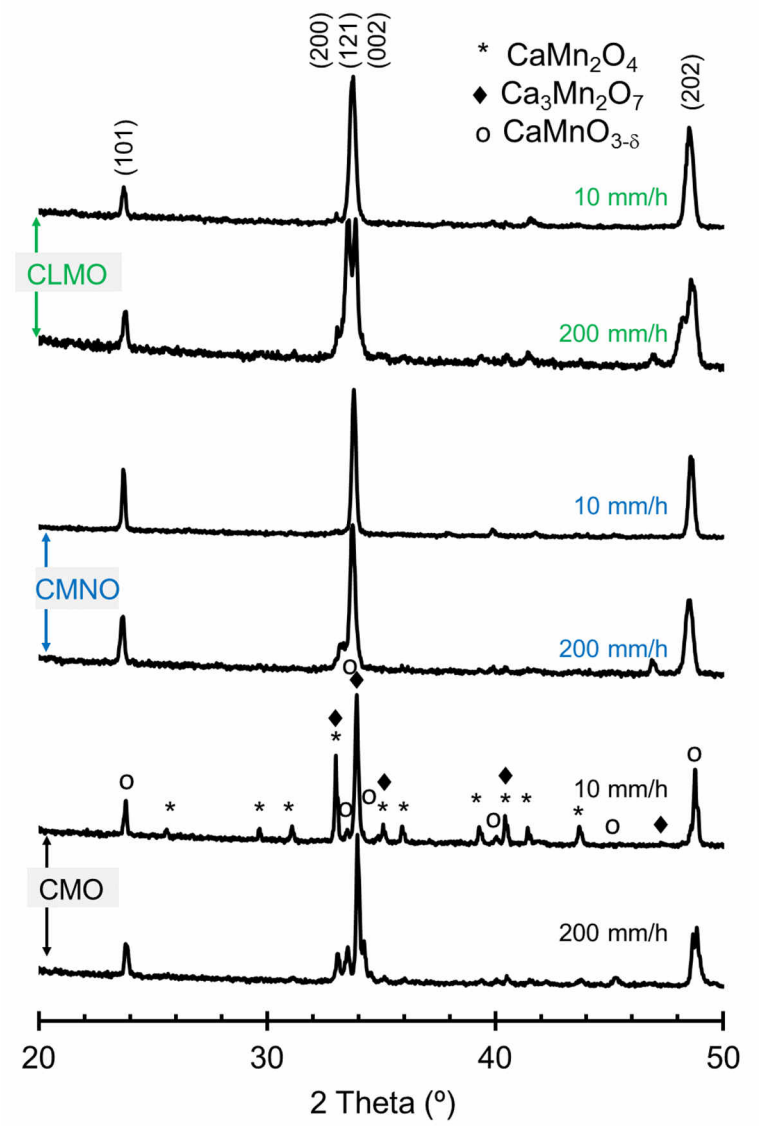

Figure 1 – Powder X-Ray diffractograms of the samples grown at different pulling rates. Diffraction planes identify the diffraction maxima associated to the $CaMnO_3$ phase. Peaks corresponding to the $CaMn_2O_4$ and $Ca_3Mn_2O_7$ secondary phases are also shown by symbols.

On the other hand, undoped samples show the opposite behaviour with the growth rate. This observation suggests that the presence of redox-stable cations like La^{3+} and Nb^{5+} may significantly affect the formation of the thermoelectric perovskite-type phase from the melt during the LFZ process. The reduction of manganese cations, further promoted by dopant cations in high oxidation states, results in coexistence of Mn^{4+} and Mn^{3+} species [24,25], which is crucial for the electronic transport. An excessive reduction leading to highly oxygen-deficient

structure in CMO samples results in structural distortions (transition from orthorhombic *Pnma* to *Pbam* space group), and the appearance of additional peaks, in excellent agreement with the literature data [23]. Such structure is apparently frozen down to ambient conditions, when high growth rate is used. On the other hand, slower growth rates lead to progressive reoxidation of the sample, resulting in subsequent phase separation, as observed in the XRD patterns. On the contrary, the presence of redox stable cations partially compensates the excessive reduction and stabilizes less-distorted *Pnma* structure. Altogether, these observations indicate a significant oxygen deficiency in the solidified materials [16,23], which is a typical consequence of the LFZ process as reported in previous works [26,27]. Furthermore, when doping with La^{3+} or Nb^{5+}, a noticeable peaks shift to lower angles in the XRD diffractograms can be observed, indicating an increase in the unit cell volume. The effect of substitution of Ca^{2+} (1.34 Å) with larger La^{3+} (1.36 Å) ions [28] is further promoted by the modification of Mn^{3+}/Mn^{4+} ratio as a charge compensation mechanism, since the ionic radius of 6-fold coordinated Mn^{3+} in both high-spin (0.645 Å) and low-spin (0.58 Å) configuration is larger than that for Mn^{4+} (0.53 Å) [28]. The same changes take place with Nb^{5+} (0.64 Å), which is larger than both Mn^{3+} and Mn^{4+} [28].

The results of morphological and chemical analysis performed by combined SEM observations and EDS mapping are shown in Fig. 2. As it can be observed from the representative micrograph taken in a longitudinal polished section, displayed in Fig. 2a (CLMO sample grown at 50 mm/h), apart from some porosity induced by the grinding procedure, no grain sizes or orientation can be determined. On the other hand, EDS maps suggest the trends in the grain orientation with respect to the growth axis, which increases when the pulling rate is raised. The above-identified phases have different Ca:Mn ratios, and are displayed as orange ($CaMnO_3$), green ($CaMn_2O_4$), and red ($Ca_3Mn_2O_7$), being in agreement with the X-ray diffraction data.

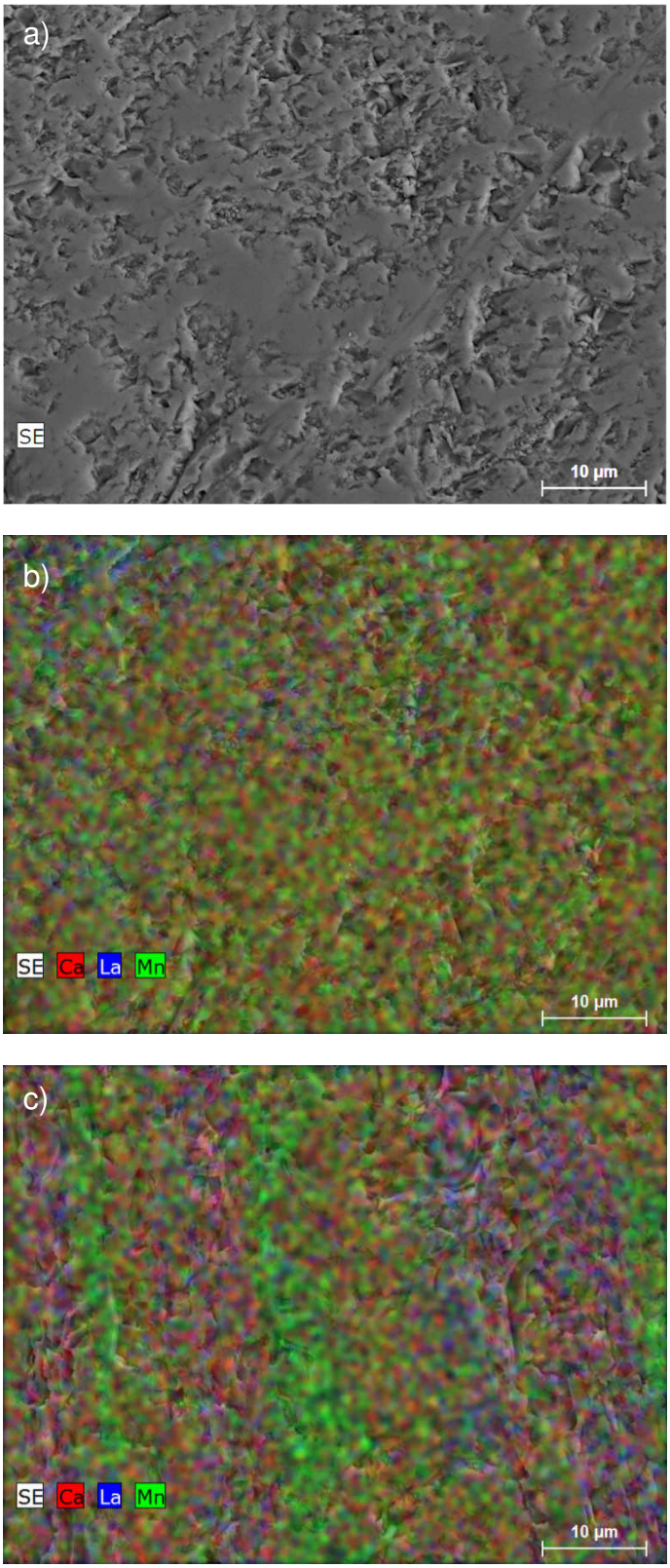

Figure 2 – a) Representative SEM micrograph of CLMO sample grown at 50 mm/h; b) and C) EDS maps of CLMO samples grown at 50 and 200 mm/h, respectively. The colors correspond to: Ca; Mn and La).

When considering the effect of the growth rate on the elements distribution, CMO and CMNO samples grown at low pulling rates show a rather uniform dispersion.

However, it is more heterogeneous when the growth rate is increased. On the other hand, CLMO samples do not show a regular evolution with the pulling rate. In these samples, the amount of Ca is lower than in the other ones (due to the partial Ca substitution by La) and the presence of $CaMn_2O_5$ phase still decreases the amount of manganese to produce the thermoelectric phase. Another effect of the pulling rate on these samples is that porosity tends to decrease by reducing the growth rate.

This evolution has been confirmed through density measurements, presented in Fig. 3. In the graph, the density evolution from the initial rods (as-extruded, indicated as 0 mm/h) to those processed by LFZ at different growth rates, is plotted, together with their measurement errors. These results are in a good agreement with the fact that LFZ process results in highly-dense materials [27]. The obtained values are close to the $CaMnO_3$ theoretical density, 4.58 g/cm^3, and to those reported in the literature [15,20]. On the other hand, the multiphasic nature of samples produced in this work complicates the estimation of the theoretical density. Moreover, doping also affects the density of the samples, increasing with La and decreasing with Nb.

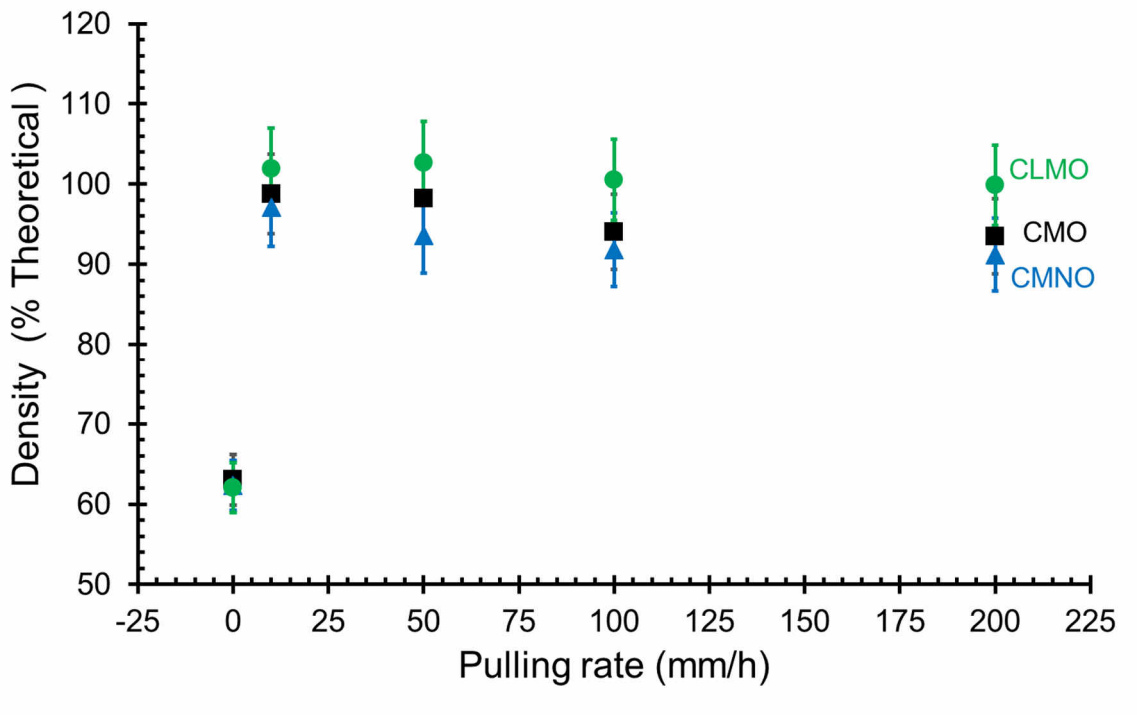

Figure 3 – Relative densities of the samples, together with their measurement error, compared to the theoretical value of $CaMnO_3$, as a function of pulling rate (0 - 200 mm/h).

Electrical resistivity as a function of temperature and growth rate is displayed in Fig. 4, together with its 4% error bars [29-31] (they are not easily seen as they are of the order of symbols size). The resistivity data do not include several samples, for which it was impossible to produce appropriate ceramics for electrical measurements due to their poor mechanical characteristics [11]. It is well-known that the charge transport in calcium manganite-based materials is generally well described by the small polaron hopping model [32]. The data show that all samples present semiconducting behaviour ($d\rho/dT < 0$) in the whole measured temperature range, which is much more evident for CMO, and CMNO samples grown at high rates. Moreover, the growth rate plays an important role on the electrical resistivity values, being lower when the growth rate is decreased, independently of the samples composition. This effect can be explained by the lower cooling rate in these samples, which allows reaching a condition closer to the equilibrium. On the other hand, La-doping drastically diminishes the effect of the growth rate on the electrical resistivity, probably due to the increase of charge carrier concentration. The minimum value at 800 ºC (9 mΩ.cm) has been determined in CLMO samples grown at 200 mm/h, which is of the order of the one obtained in electron-doped materials (10-12 mΩ.cm) [12,33,34], prepared using much longer processing time.

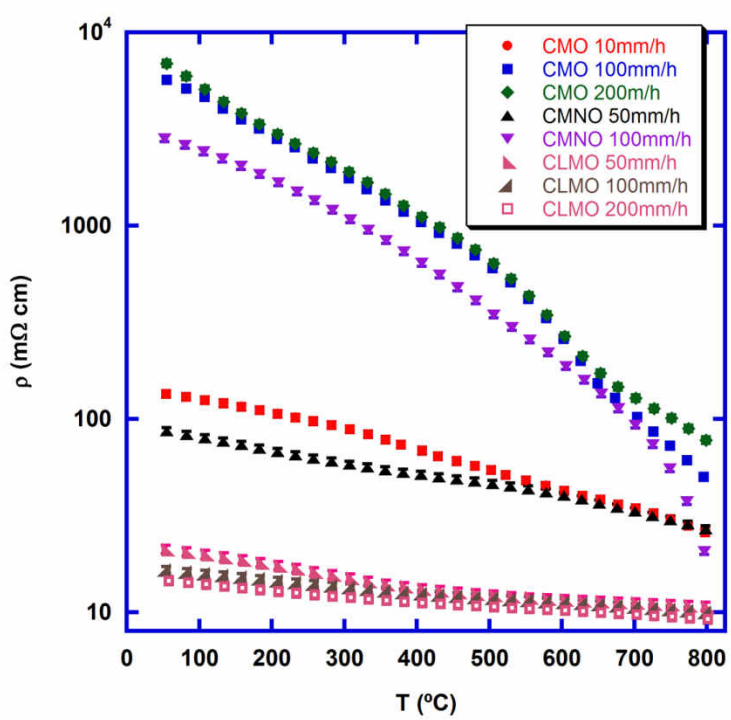

Figure 4 – Electrical resistivity evolution with temperature, together with its error, as a function of the growth rate and composition.

Evolution of the Seebeck coefficient with temperature for all samples, together with corresponding 4 % uncertainty [29-31], is presented in Fig. 5. As it can be observed from the graph, the values of S are negative in the whole measured temperature range, indicating that the main transport charge carriers are electrons. Undoped $CaMnO_3$ samples show very high |S| values, which are decreasing when the temperature is raised. This behaviour can be associated to their low carrier concentration, reflected in the semiconducting behaviour observed for the electrical resistivity. Moreover, doped materials possess lower |S| values at room temperature, which are increasing on heating. These results are in agreement with those obtained in other works studying the effect of transition metal substitutions on the thermoelectric properties of $CaMnO_3$ [7,22,35]. The highest |S| values at 800 ºC, for the doped materials, have been measured in CMNO samples grown at 50 mm/h (~ 190 μV/K), which are around the best obtained in electron doped materials prepared through different techniques (140-250 μV/K) [6,12,32-34].

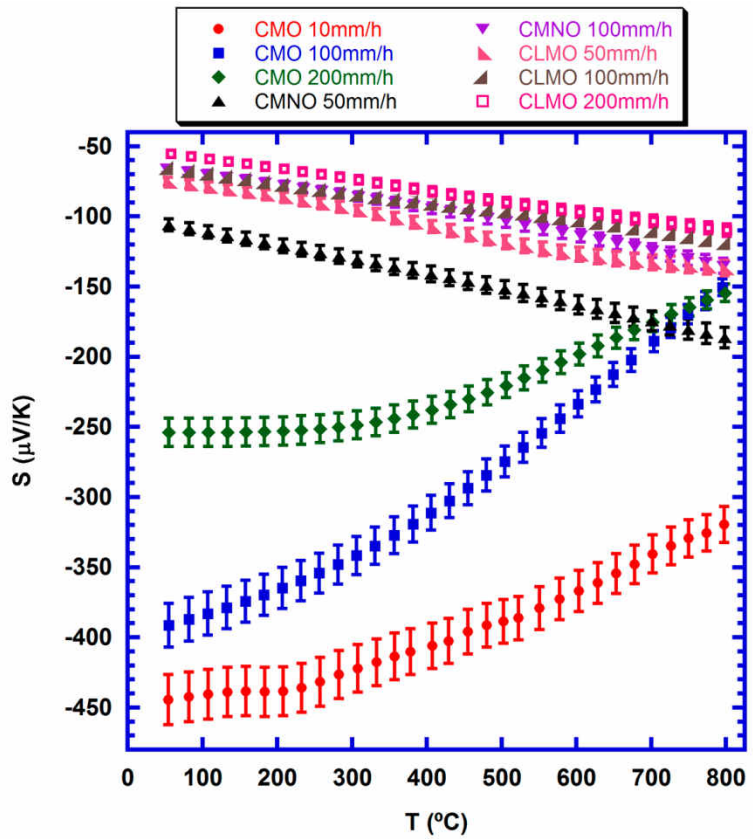

Figure 5 –Evolution of the Seebeck coeficient with temperature, together with its corresponding error, as a function of the growth rate and composition.

Fig. 6 shows the thermoelectric performance (power factor) of all fibers, together with the corresponding uncertainty (10 %) [36]. Lower growth rates lead to the highest PF values, independently of the samples composition. This effect, as mentioned in the electrical resistivity discussion, is due to the lower cooling rate these samples during the growth process. On the other hand, La-doped samples show better performances than the Nb-containing materials, due to their most effective electron doping. Surprisingly, the highest PF values have been obtained in undoped samples grown at 10 mm/h in the whole measured temperature range. These results clearly point out to even rather important effect of the growth rates on the performances than the doping itself. The maximum value at 800 ºC (0.39 mW/K^{2}m), obtained in undoped samples, is higher than the reported in the literature for doped materials 0.17-0.37 mW/K^{2}m [6,33,34,37].

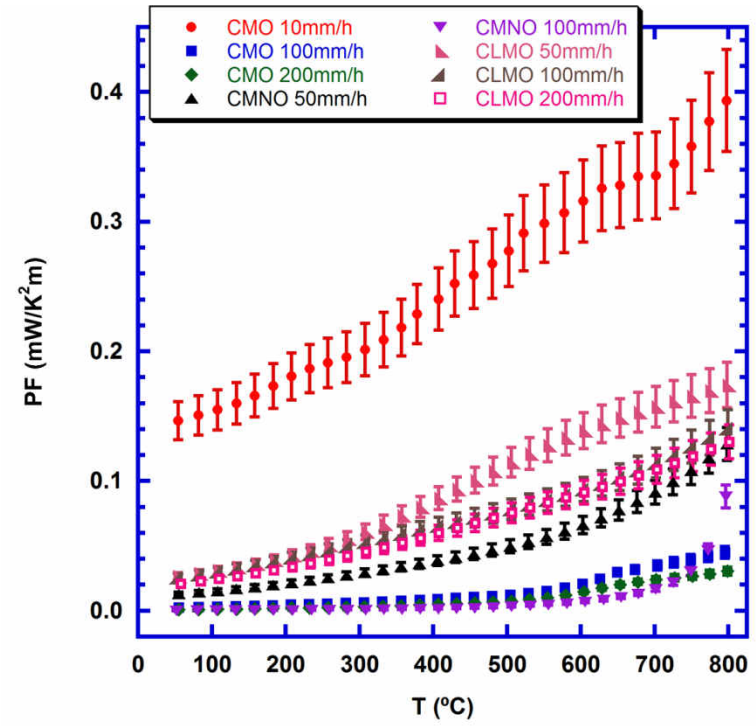

Figure 6 –Power factor evolution with temperature, together with its corresponding error, as a function of the growth rate and composition.

The effect of doping on the PF values at high temperatures (800 ºC) can be clearly observed when presenting these data as a function of the growth rate (Fig. 7). In general, CLMO samples show the highest thermoelectric performances, when compared to the samples grown at the same rates. Moreover, the lowest performances are obtained, as expected, in undoped samples. On the other hand, when considering the effect of the pulling rate on the samples performances, it is clear that they are slightly increased when the growth rate is decreasing from 200 to 100 mm/h. This evolution is maintained for the lower pulling rates, but the raise in performances is nearly exponential for very low growth rates (10 mm/h). The reasons for this behaviour are still not clear. In particular, it might be related to a favourable interplay between charge and electron spin states in these samples. In any case, further detailed studies are necessary in order to clarify the mechanism behind these properties.

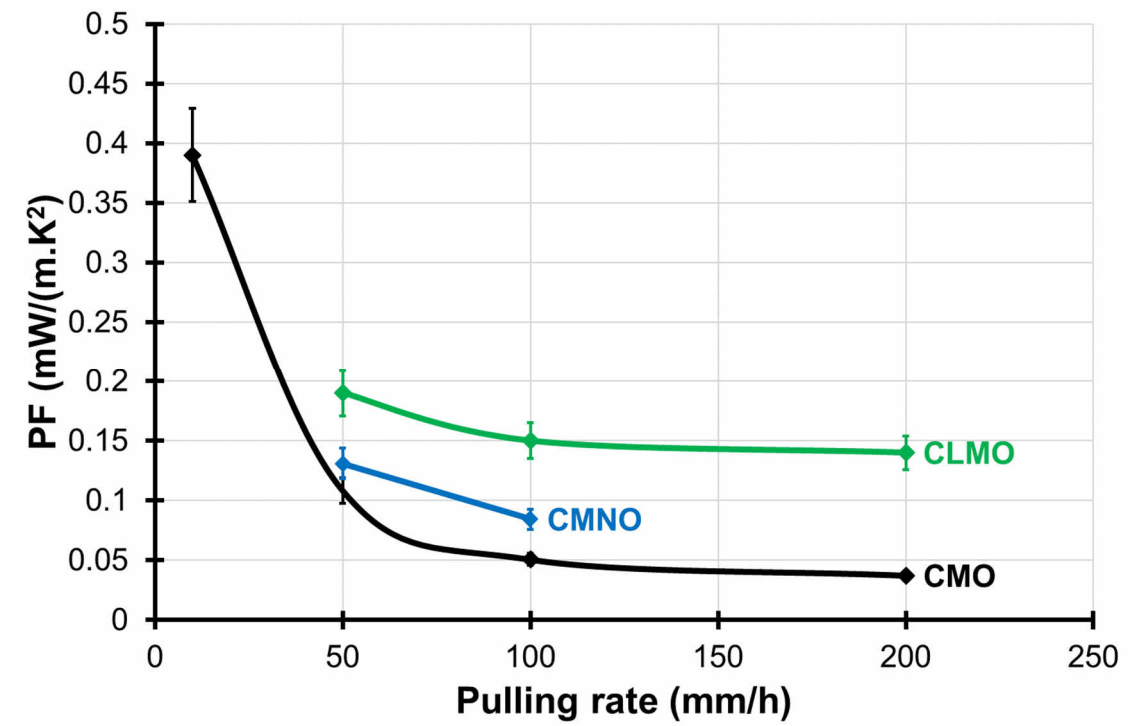

Figure 7 – Evolution of the power factor with the pulling rate at 800ºC, together with its uncertainty, as a function of composition.

Conclusions

In the scope of this work, pure and electron-doped $CaMnO_3$ samples were processed through the LFZ technique using different pulling rates from 10 to 200 mm/h. XRD analysis showed the presence of perovskite-type phase as the major one in all samples. The appearance of secondary $CaMn_2O_4$ and $Ca_3Mn_2O_7$ phases has been partially suppressed by using slower pulling rates. The presence of redox-stable cations like La^{3+} and Nb^{5+} appears to stabilize the Pnma orthorhombic perovskite phase, while highly oxygen-deficient Pbam structure is formed in the case of undoped $CaMnO_3$. The lowest resistivity at 800ºC was obtained for La-doped samples grown at 200 mm/h (9 mΩ.cm). On the other hand, the highest Seebeck coefficient (320 µV/K at 800 ºC) has been determined in undoped samples grown at 10 mm/h. This value, combined with relatively low electrical resistivity, resulted in exceptionally high PF (~0.39 mW/K^{2}m at 800ºC), one of the highest reported so far in the literature. However, further improvements can be achieved if successful growth of doped samples at very low pulling rates can be performed. Moreover, evaluation of the thermal conductivity should

provide a real assessment of the thermoelectric performances of these samples. In any case, the LFZ technique can be regarded as a very useful process to produce thermoelectric legs for power generation modules in just one step.

Acknowledgements:

The authors are grateful to i3N (FCT UID/CTM/50025/2019), CICECO-Aveiro Institute of Materials (FCT UID/CTM/50011/2019) and project POCI-01-0145-FEDER-031875, financed by COMPETE 2020 Program and national funds through the FCT/MEC and FEDER under the PT2020 Partnership Agreement. NMF thanks FCT for the grant SFRH/BPD/111460/2015. AK acknowledges the support of the project of bilateral cooperation between FCT and DAAD (Germany). M. A. Madre, M. A. Torres, and A. Sotelo acknowledge Gobierno de Aragón-FEDER (Research Group T 54-17R), and MINECO-FEDER (Project MAT2017-82183-C3-1-R) for financial support.

References

[1] R. He, S. Gahlawat, Studies on mechanical properties of thermoelectric materials by nanoindentation, Phys. Status Solidi 212 (2015) 2191–2195.

[2] M. Demir, I. Dincer, Performance assessment of a thermoelectric generator applied to exhaust waste heat recovery, Appl. Thermal Eng. 120 (2017) 694-707.

[3] T. Seetawan, K. Singsoog, Thermoelectric Energy Conversion of p-$Ca_3Co_4O_9$/n-$CaMnO_3$ Module, Energ. Proc. 61 (2014) 1067-1070.

[4] P. Phaga, A. Vora-Uda, Invention of Low Cost Thermoelectric Generators, Proc. Eng. 32 (2012) 1050-1053.

[5] A. V. Kovalevsky, A. A. Yaremchenko, S. Populoh, A. Weidenkaff, J. R. Frade, Enhancement of Thermoelectric Performance in Strontium Titanate by Praseodymium Substitution, J. Appl. Phys. 113 (2013) 053704-8.

[6] R. Kabir, R. Tian, Role of Bi doping in thermoelectric properties of $CaMnO_3$, J. Alloys Compds. 628 (2015) 347-351.

[7] H. Wang, W. Su, J. Liu, C. Wang, Recent development of n-type perovskite thermoelectrics, J Materiomics 2 (2016) 225–236, doi: 10.1016/j.jmat.2016.06.005

[8] R. Kabir, D. Wang, T. Zhanga, R. Tian, R. Donelson, T. T. Tan, S. Li, Tunable thermoelectric properties of $Ca_{0.9}Yb_{0.1}MnO_3$ through controlling the particle size via ball mill processing, Ceram. Int. 40 (2014) 16701–16706, doi: 10.1016/j.ceramint.2014.08.033

[9] A. Sotelo, M. A. Torres, M. A. Madre, J. C. Diez, Effect of synthesis process on the densification, microstructure, and electrical properties of $Ca_{0.9}Yb_{0.1}MnO_3$ ceramics, Int. J. Appl. Ceram. Technol. 14, 1190-1196 (2017), doi: 10.1111/ijac.12711

[10] N. M. Ferreira, M. C. Ferro, A. R. Sarabando, A. Ribeiro, A. Davarpanah, V. Amaral, M. A. Madre, A. V. Kovalevsky, M. A. Torres, F. M. Costa, A. Sotelo, Improvement of thermoelectric properties of $Ca_{0.9}Gd_{0.1}MnO_3$ by powder engineering through K_2CO_3 additions, J Mater Sci. 54 (2019), 3252-3261, doi: 10.1007/s10853-018-3058-x

[11] M. Molinari, D. Tompsett, Structural, electronic and thermoelectric behaviour of $CaMnO_3$ and $CaMnO_{3-\delta}$, J. Mater. Chem. A 2 (2014) 14109-14117, doi: 10.1039/c4ta01514b

[12] D. Flahaut, T. Mihara, R. Funahashi, N. Nabeshima, K. Lee, H. Ohta, K. Koumoto, Thermoelectrical properties of A-site substituted $Ca_{1-x}Re_xMnO_3$ system, J. Appl. Phys. 100 (2006) 084911.

[13] Y. Wang, Y. Sui, High temperature thermoelectric response of electron-doped $CaMnO_3$, Chem. Mater. 21 (2009) 4653–4660.

[14] A. Zevalkink, D. M. Smiadak, J. L. Blackburn, A. J. Ferguson, M. L. Chabinyc, O. Delaire, J. Wang, K. Kovnir, J. Martin, L. T. Schelhas, T. D. Sparks, S. D. Kang, M. T. Dylla, G. J. Snyder, B. R. Ortiz, E. S. Toberer, A practical field guide to thermoelectrics: Fundamentals, synthesis, and characterization, Appl. Phys. Rev. 5 (2018) 021303; doi: 10.1063/1.5021094

[15] Y. Wang, Y. Sui, X. Wang, Thermal conductivity of electron-doped $CaMnO_3$ perovskites: Local lattice distortions and optical phonon thermal excitation, Acta Mater. 58 (2010) 6306-6316.

[16] L. Bocher, M. H. Aguirre, R. Robert, D. Logvinovich, S. Bakardjieva, J. Hejtmanek, A. Weidenkaff, High-temperature stability, structure and thermoelectric properties of $CaMn_{1-x}Nb_xO_3$ phases, Acta Materialia 57 (2009) 5667

[17] N. M. Ferreira, A. V. Kovalevsky, M. A. Valente, N. A. Sobolev, J. C. Waerenborgh, F. M. Costa, J. R. Frade, Iron incorporation into magnesium aluminosilicate glass network under fast laser floating zone processing, Ceram. Int. 42 (2016) 2693-2698, doi: 10.1016/j.ceramint.2015.10.150.

[18] R. A. Silva, F. M. Costa, R.F. Silva, J. P. Andreeta, A. C. Hernandes, Electric field-modified segregation in crystal fibers of colossal magnetoresistive La0.7Ca0.3MnO3, Journal of Crystal Growth, 310 (2008) 3568– 3572, doi: 10.1016/j.jcrysgro.2008.04.003.

[19] M. A. Madre, F. M. Costa, N. M. Ferreira, A. Sotelo, M. A. Torres, G. Constantinescu, Sh. Rasekh, J. C. Diez, Preparation of high-performance $Ca_3Co_4O_9$ thermoelectric ceramics produced by a new two-step method, J. Eur. Ceram. Soc. 33 (2013) 1747–1754. DOI: 10.1016/j.jeurceramsoc.2013.01.029

[20] R. Lohnert, M. Stelter, J. Topfer, Evaluation of soft chemistry methods to synthesize Gd-doped $CaMnO_{3-\delta}$ with improved thermoelectric properties, Mater. Sci. Eng. B 223 (2017) 185–193. Doi: 10.1016/j.mseb.2017.06.014

[21] H. S. Horowitzm, J. M. Longo, Phase relations in the Ca-Mn-O system. Mater. Res. Bull. 13 (1978) 1359–1369.

[22] J. W. Park, D. H. Kwak, S. H. Yoon, S. C. Choi, Thermoelectric properties of Bi, Nb co-substituted $CaMnO_3$ at high temperature, J. Alloys Compds. 487 (2009) 550–555.

[23] J. Du, T. Zhang, F. Cheng, W. Chu, Z. Wu, J. Chen, Nonstoichiometric Perovskite $CaMnO_{3-\delta}$ for Oxygen Electrocatalysis with High Activity, Inorg. Chem. 53 (2014) 9106–9114, doi: 10.1021/ic501631h

[24] J. M. Alonso, J. M. González-Calbet, A. Hernando, M. Vallet-Regí, M. E. Dávila, M. C. Asensio, Influence of Mn^{2+} in the magnetic behaviour of manganese related-perovskites, J. Phys. Chem. Solids 67 (2006) 571–574, doi:10.1016/j.jpcs.2005.10.159

[25] L. Ruiz-González, R. Cortés-Gil, J. M. Alonso, J. M. González-Calbet, M. Vallet-Regí, Revisiting the Role of Vacancies in Manganese Related Perovskites, Open Inorg. Chem. J. 1 (2007) 37-46

[26] N. M. Ferreira, A. Kovalevsky, M. A. Valente, F. M. Costa, and J. Frade, Magnetite/Hematite Core/Shell Fibres Grown by Laser Floating Zone Method, Appl. Surf. Sci., 278 (2013) 203–206, doi: 10.1016/j.apsusc.2013.01.108

[27] N. M. Ferreira, A. V. Kovalevsky, F. M. Costa, J. R. Frade, Processing effects on properties of $(Fe,Mg,Al)_3O_4$ Spinels as Potential Consumable Anodes for Pyroelectrolysis, J. Am. Ceram. Soc. 99 (2016) 1–5, DOI: 10.1111/jace.14190

[28] R. D. Shannon, Revised Effective Ionic Radii and Systematic Studies of Interatomic Distances in Halides and Chalcogenides, Acta Cryst. A 32 (1976) 751-767.

[29] A. Sotelo, F. M. Costa, N. M. Ferreira, A. Kovalevsky, M. C. Ferro, V. S. Amaral, J. S. Amaral, Sh. Rasekh, M. A. Torres, M. A. Madre, J. C. Diez, *Tailoring $Ca_3Co_4O_9$ microstructure and performances using atransient liquid phase sintering additive*, J. Eur. Ceram. Soc. 36 (2016) 1025-1032.

[30] S. Populoh, M. H. Aguirre, O. C. Brunko, K. Galazka, Y. Lu, A. Weidenkaff, High figure of merit in (Ti,Zr,Hf)NiSn half-Heusler alloys, Scr. Mater. 66 (2012) 1073-1076.

[31] B. Ozcelik, G. Cetin, M. Gursul, M. A. Madre, A. Sotelo, S. Adachi, Y. Takano, Low Temperature Thermoelectric Properties of K-Substituted $Bi_2Sr_2Co_2O_y$ Ceramics Prepared via Laser Floating Zone Technique, J. Eur. Ceram. Soc. 2019. DOI: 10.1016/j.jeurceramsoc.2019.04.029

[32] L. Bocher, M. H. Aguirre, D. Logvinovich, A. Shkabko, R. Robert, M. Trottmann, A. Weidenkaff, $CaMn_{1-x}Nb_xO_3$ (x = 0.08) Perovskite-Type Phases As Promising New High-Temperature n-Type Thermoelectric Materials, Inorg. Chem. 47 (2008) 8077-8085.

[33] M. Mouyane, B. Itaalit, Flash Combustion Synthesis of electron doped-$CaMnO_3$ thermoelectric oxides, Powder Technol. 264 (2014) 71-77.

[34] Y. C. Zhou, C. L. Wang, W. B. Su, J. Liu, H. C. Wang, J. C. Li, Y. Li, J. Z. Zhai, Y. C. Zhang, L. M. Mei, Electrical properties of Dy^{3+}/Na^{+} Co-doped oxide thermoelectric $[Ca_{1-x}(Na_{1/2}Dy_{1/2})_x]MnO_3$ ceramics, J. Alloys Compds. 680 (2016) 129-132. Doi: 10.1016/j.jallcom.2016.04.158

[35] N. M. Mazur, Microstructural design of $CaMnO_3$ and its thermoelectric proprieties, Norwegian University of Science and Technology (NTNU), June 2015, https://core.ac.uk/download/pdf/154669141.pdf (seen at Nov2018)

[36] D. Flahaut, J. Allouche, A. Sotelo, Sh. Rasekh, M. A. Torres, M. A. Madre, J.C. Diez, Role of Ag in textured-annealed $Bi_2Ca_2Co_{1.7}O_x$ thermoelectric ceramic, Acta Mater. 102 (2016) 273-283.

[37] H. C. Wang, C. L. Wang, Synthesis of Dy doped $Yb_{0.1}Ca_{0.9}MnO_3$ ceramics with a high relative density and their thermoelectric properties, Mater. Res. Bull. 47 (2012) 2252–2256. Doi: 10.1016/j.materresbull.2012.05.061